Alexandria Engineering Journal (2022) 61, 2030–2044

Alexandria University

Alexandria Engineering Journal

www.elsevier.com/locate/aej
www.sciencedirect.com

A new artificial ecosystem-based optimization integrated with Nelder-Mead method for PID controller design of buck converter

Davut Izci [a], **Baran Hekimoğlu** [b], **Serdar Ekinci** [c,*]

[a] *Department of Electronics & Automation, Batman University, Batman 72060 Turkey*
[b] *Department of Electrical & Electronics Engineering, Batman University, Batman 72100 Turkey*
[c] *Department of Computer Engineering, Batman University, Batman 72100, Turkey*

Received 3 January 2021; revised 12 April 2021; accepted 18 July 2021
Available online 07 August 2021

KEYWORDS

Artificial ecosystem-based optimization;
Nelder-Mead method;
PID controller;
Buck converter

Abstract Over the last decade, there has been a constant development in control techniques for DC-DC power converters which can be classified as linear and nonlinear. Researchers focus on obtaining maximum efficiency using linear control techniques to avoid complexity although nonlinear control techniques may achieve full dynamic capabilities of the converter. This paper has a similar purpose in which a novel hybrid metaheuristic optimization algorithm (AEONM) is proposed to design an optimal PID controller for DC-DC buck converter's output voltage regulation. The AEONM employs artificial ecosystem-based optimization (AEO) algorithm with Nelder-Mead (NM) simplex method to ensure optimal PID controller parameters are efficiently tuned to control output voltage of the buck converter. Initial evaluations are performed on benchmark functions. Then, the performance of AEONM-based PID is validated through comparative results of statistical boxplot, non-parametric test, transient response, frequency response, time-domain integral-error-performance indices, disturbance rejection and robustness using AEO, particle swarm optimization and differential evolution. A comparative performance analysis of transient and frequency responses is also performed against simulated annealing, whale optimization and genetic algorithms for further performance assessment. The comparisons have shown the proposed hybrid AEONM algorithm to be superior in terms of enhancing the buck converter's transient and frequency responses.

1. Introduction

The widespread application of DC-DC power converters in different fields, such as renewable energy, electric vehicle, consumer electronics, etc., have created an increased demand for improved dynamic performance, stability and regulation accu-

* Corresponding author.
E-mail addresses: davut.izci@batman.edu.tr (D. Izci), baran.hekimoglu@batman.edu.tr (B. Hekimoğlu), serdar.ekinci@batman.edu.tr (S. Ekinci).

Peer review under responsibility of Faculty of Engineering, Alexandria University.

https://doi.org/10.1016/j.aej.2021.07.037

racy of switching mode power supplies (SMPS) by advanced control methods [1]. Various control strategies, ranging from relatively simple structures to more advanced types, have been proposed to enhance the performance of DC-DC converters. Type-II, Type-III, proportional-integral (PI) and proportional-integral-derivative (PID) controllers are only few examples of widely adopted control techniques for performance enhancement. It is worth to note that, Type-II controllers are characterized by having one zero and two poles (one pole at the origin and the other at a higher frequency) and they are mostly used with current-mode control of DC-DC converters whereas Type-III controllers require additional one zero and one pole and they are generally used with voltage-mode control [2].

More advanced control methods are also available for the same purpose apart from the above listed structures. The advanced control techniques employed for the same purpose can be listed as fractional order PID (FOPID) control, fuzzy logic control (FLC), linear quadratic regulator (LQR), model predictive control (MPC), deadbeat control (DBC), switching boundary control (SBC), sliding mode control (SMC), time optimal control (TOC) and passivity-based control (PBC) [3,4]. These control techniques can be classified broadly into linear and nonlinear control methods and they play an important role in affecting performance of power converters since the latter structures are considered as the center part in SMPS design [5]. Hence, it is important to choose a suitable controller to reach the desired design goals without increasing the control system complexity.

Despite having limited bandwidths, small-signal based linear control design approaches such as PI and PID controllers are still being investigated as part of the ongoing research studies about performance improvement. It is well known that a properly tuned PID controller can achieve the following objectives with less computational burden [4]; (1) closed-loop stability over the target operating range, (2) fast transient recovery, (3) robustness against parameter variations and model uncertainty and (4) acceptable noise attenuation. However, these objectives cannot be fully achieved by conventional tuning methods such as Ziegler-Nichols (ZN), Cohen-Coon (CC), gain- and phase-margin, or pole placement.

Many studies related to optimization of linear controller parameters for DC-DC power converters have shown the effectiveness of metaheuristic algorithms in reaching the abovementioned objectives. For example, PI and Type-III controllers have been designed for a non-inverting buck-boost converter by utilizing ant colony algorithm (ACO) [6]. The performance of those controllers was compared with the controllers tuned by a classical method based on a conventional frequency response technique. Both simulation and experimental results have shown the effectiveness of ACO based controller designs in terms of frequency domain performance indices. The capability of metaheuristic based approaches has also been shown for transient response enhancement by stabilizing output voltage of a basic inverting buck-boost converter via bacterial foraging optimization (BFO) based PI controller [7] which clearly demonstrated the better performance. Further PI controller design examples have been reported for a two-loop boost converter based power factor correction (PFC) circuit using genetic algorithm (GA), particle swarm optimization (PSO) and differential evolution (DE) algorithm [8]. In the latter reported work, metaheuristic approaches were shown to perform better not only in response to line/load variations but also in terms of program size, complexity, and convergence time. One of the latter listed algorithms (PSO) has also been used for achieving an optimum Type-III controller employed for both boost converter and interleaved boost converter (IBC) [9]. Likewise, the performance comparison has been performed against conventional techniques and the best closed loop performance, the largest stability margin, and the highest system bandwidth were achieved via metaheuristic approach. Examples of metaheuristic approaches are also available for PID controller design, as well, which is adopted in power converters. Hybrid whale optimization algorithm (WOA) with simulated annealing (SA) [10] and hybrid firefly algorithm (FA) with PSO algorithm [11] can be listed as some of those examples. The optimization algorithms given above for the control of DC-DC converters contain only a small portion of their usage in the field of engineering. Metaheuristic methods have been gaining an increased popularity as an alternative in engineering applications since traditional optimization techniques are possessing disadvantages [12].

Artificial ecosystem-based optimization (AEO) algorithm is one of those metaheuristic algorithms, which is inspired from nature [13], proposed to deal with optimization problems as an alternative to existing approaches. Several real-world engineering applications have already employed AEO algorithm such as parameter identification of different configurations of photovoltaic (PV) models [14], parameter extraction of different electrolyte membrane fuel cell stack models [15] and proton exchange membrane fuel cells model [16], detection of tuberculosis in chest radiographs [17], allocation of multiple distributed generations [18], solution of large-scale reactive power dispatch problem [19] along with configuration of a hybrid photovoltaic, wind turbine and fuel cell (PV/WT/FC) energy system [20]. AEO algorithm exhibits poor exploitation, despite its abovementioned applications, because of its stochastic nature. To deal with this issue and increase the exploitation capability of AEO algorithm, Nelder-Mead (NM) simplex method can be adopted.

The latter method has a history of more than five decades which was proposed to deal with the minimization problems [21]. It has been already combined with several algorithms for enhancing the capability. Recently reported examples of improved algorithms using NM can be listed as BFO algorithm for solving economic dispatch problem [22], DE algorithm for parameter identification of chaotic systems [23], FA algorithm for solution of reactive power dispatch problem [24], gravitational search algorithm (GSA) for optimization of thin-wall structures [25], cuckoo search (CS) algorithm for optimization of renewable based generations in AC-DC microgrid system [26], Jaya algorithm for parameter estimation of proton exchange membrane fuel cells [27], Harris hawks optimization (HHO) algorithm for solutions of design and manufacturing problems [28], dragonfly algorithm (DA) for training multilayer perceptron [29], hybrid PSO and sine cosine algorithm (SCA) for solution of engineering design problems [30] and artificial electric field (AEF) algorithm for optimization of benchmark problems [12].

In this paper, an improved AEO algorithm has been constructed by utilization of NM method. The improved algorithm, named as AEONM algorithm, was used for parameter tuning of a PID controller in a DC-DC buck converter. State-of-the-art algorithms have been adopted for com-

paring the obtained results. The latter evaluation showed the proposed AEONM algorithm to be superior to other algorithms in terms of efficiency and performance. The contributions of this study to the literature can be summarized as follows:

i. The hybrid AEONM algorithm is proposed for the first time to exploit the AEO's good global search ability and NM's good local search capability.
ii. The performance evaluation on six well-known benchmark functions has demonstrated greater success of the proposed algorithm in terms of achieving the statistical metrics of best, mean and standard deviation.
iii. The proposed hybrid AEONM algorithm and original AEO algorithm are both used for the first time in PID controller design for a DC-DC buck converter system. This is the first application of AEO and AEONM algorithms in the power electronics field.
iv. The efficiency of the proposed hybrid AEONM based PID controller, designed for further performance improvement of DC-DC buck converter, has been validated through various analyzes such as statistical boxplot, non-parametric test, transient response, frequency response, time-domain integral-error-performance indices, disturbance rejection and robustness through comparing with the original AEO algorithm and other commonly used well-known successful algorithms such as PSO and DE.
v. Further performance demonstration of the AEONM based PID controller for DC-DC buck converter in terms of transient and frequency responses was performed via comparing it with other state-of-the-art algorithms (SA, GA and WOA) based PID controllers used for the same purpose.

The organization for the rest of the paper is as follows; Section 2 and 3 introduce AEO algorithm and NM simplex method, respectively. The proposed hybrid AEONM algorithm is given in Section 4 whereas Section 5 describes the basic operation and modeling of DC–DC buck converter. PID controlled buck converter is also provided in the latter section. Section 6 defines the optimization problem with the proposed design approach. Section 7 discusses simulation results with detailed comparisons using statistical boxplot analysis, non-parametric test analysis, transient response analysis, frequency response analysis, and time domain based integral-error performance indices. The disturbance rejection performance of DC-DC buck converter is also presented in the latter section. Finally, Section 8 concludes the overall work.

2. Artificial ecosystem-based optimization

The ecosystem concept, introduced in 50 s, has inspired the development of artificial ecosystem-based optimization (AEO) algorithm as a novel nature-inspired metaheuristic approach [13]. This basically is an algorithm that relies on the energy transfer mechanism between living organisms which helps maintaining the stability of species. To do so, three operators, named as production, consumption and decomposition, are employed to achieve solutions. Fig. 1 demonstrates the energy flow in an ecosystem that has producer, consumer and decomposer.

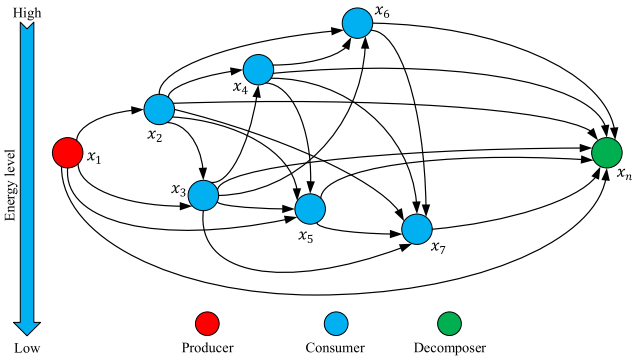

Fig. 1 An ecosystem in AEO.

2.1. Production

In AEO, the worst individual of the population is represented by the producer. Therefore, it requires to be updated with respect to the best individual by considering the upper and lower limits of the search space so that it can help other individuals to search for other regions. A new individual is produced, via the production operator, between the best (x_n) and a randomly generated (x_{rand}) individuals by replacing the previous one. The production operator's mathematical representation is given as follows:

$$x_1(t+1) = (1-\alpha)x_n(t) + \alpha x_{rand}(t) \tag{1}$$

$$\alpha = (1 - t/T)r_1 \tag{2}$$

$$x_{rand} = \bar{r}\,(Ub - Lb) + Lb \tag{3}$$

where the population size is denoted by n, maximum iteration number is T, upper limit is Ub, lower limit is Lb and a random number ranging between $[0, 1]$ is r_1. α and $\bar{r}$ represent a linear weight coefficient and a random vector having a range of $[0, 1]$, respectively. The α coefficient given in Eq. (1) helps drifting the individual linearly from a random position towards the best individual through iterations.

2.2. Consumption

This operator is performed by the consumers after the production operator finishes the producers. A randomly chosen consumer having lower energy or a producer may be eaten by each consumer in order to obtain energy. A Lévy flight-like random walk, named as consumption factor (C), is defined as follows in order to enhance the exploration capability:

$$C = \frac{1}{2}\frac{v_1}{|v_2|} \tag{4}$$

$$v_1 \sim N(0,1), v_2 \sim N(0,1) \tag{5}$$

where $N(0, 1)$ represents a normal distribution such that the mean and the standard deviation equal to 0 and 1, respectively. Different strategies are adopted by different types of consumers. A consumer would only eat the producer in case of

being randomly chosen as an herbivore (see Fig. 1 – x_2 and x_5 are herbivore consumers, thus, only eat the producer x_1). The herbivore consumption behavior is modelled mathematically as in Eq. (6).

$$x_i(t+1) = x_i(t) + C \cdot (x_i(t) - x_1(t)), i \in [2, \cdots, n] \tag{6}$$

A consumer would only eat another consumer with higher level of energy if it is chosen as a carnivore randomly (see Fig. 1 – A consumer from individuals of x_2 to x_5 are eaten by the consumer x_6 as the latter is a carnivore and has a lower energy level than those individuals of x_2 to x_5). A carnivore behavior is modelled as:

$$x_i(t+1) = x_i(t) + C \cdot \big(x_i(t) - x_j(t)\big), i \in [3, \cdots, n]$$

$$j = randi([2\ i-1]) \tag{7}$$

Unlike the latter two behavior, a consumer with a higher energy level or a producer can randomly be eaten by the consumer if it is chosen as an omnivore randomly (see Fig. 1 – Both the producer x_1 and a randomly chosen consumer from x_2 to x_6 can be eaten by x_7 since it is an omnivore and has lower level of energy than x_2 to x_6). The mathematical form of this behavior is expressed as:

$$x_i(t+1) = x_i(t) + C \cdot (r_2 \cdot (x_i(t) - x_1(t))) + (1 - r_2)\big(x_i(t) - x_j(t)\big), i \in [3, \cdots, n]$$

$$j = randi([2\ i-1]) \tag{8}$$

where r_2 denotes a random number of $[0, 1]$ range. A search individual's position is updated with respect to either a randomly chosen or the worst individuals in a population using the consumption operator. This, therefore, allows the algorithm to perform a global search.

2.3. Decomposition

This is an of crucial process in order to have an appropriately working ecosystem. The decomposer chemically breaks down the remains of each died individual in the population in order to provide required nutrients for the producer's growth. The weight coefficients of h and e along with the decomposition factor of D are designed to model this behavior mathematically. Those parameters help updating the position of x_i (*ith* individual) by the position of x_n (the decomposer's position). Also, each individual's next position is allowed to spread around the decomposer (best individual). The mathematical expression is given as follows:

$$x_i(t+1) = x_n(t) + D \cdot (e \cdot x_n(t) - h \cdot x_i(t)), i \in 1, \cdots, n \tag{9}$$

$$D = 3u, u \sim\ N(0, 1) \tag{10}$$

$$e = r_3 \cdot randi([1\ 2]) - 1 \tag{11}$$

$$h = 2 \cdot r_3 - 1 \tag{12}$$

To sum up the algorithm briefly, a random population is generated at first and through each iteration, the position of the first individual is updated using Eq. (1). The positions of other individuals are updated by choosing amongst Eqs. (6)–(8) with the same probability. Each individual updates its position using Eq. (9) in case of an individual having a better function value. An individual is generated randomly in the search space if it goes beyond the upper and lower boundaries. This continues until a satisfactory termination criterion is met. The final step returns the best individual found so far. The flowchart that provides entire steps of the basic AEO algorithm is given in Fig. 2.

3. Nelder-Mead method

This algorithm is simplex method and has been developed to solve non-linear functions via gradient-free computations [21]. An optimal vertex (x_1) is identified through generating $d+1$ vertices ($x_1, x_2, \ldots x_{d+1}$) and evaluating the respective fitness function values ($f(x_1), f(x_2), \ldots, f(x_{d+1})$). The evaluated fitness functions are then compared and sorted in ascending order. Following the latter adjustment, four scalar coefficients named as reflection (ρ), expansion (γ), contraction (β) and

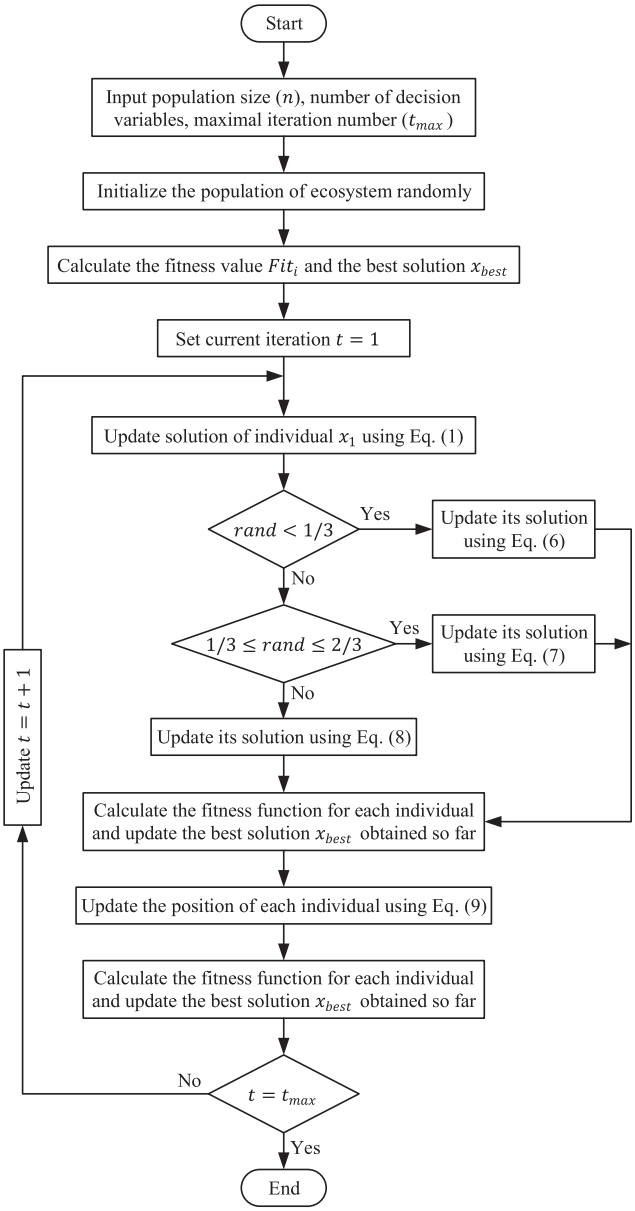

Fig. 2 Flowchart of the basic AEO algorithm.

shrinkage (δ) are used to replace the worst vertex (x_{d+1}) with a new one. Those parameters must be specified such that the relationship of $\rho > 0$, $\gamma > 1$, $\gamma > \rho$, $0 < \beta < 1$ and $0 < \delta < 1$ should be satisfied [31]. The respective values chosen for this study for the stated parameters are provided in Section 7.1.

After initial arrangement, the computed fitness values are sorted to establish the best (x_1), the worst (x_{d+1}) and the centroid ($\bar{x}$) points. Then, Eq. (13) is used to identify the reflection point (x_r):

$$x_r = \bar{x} + \rho(\bar{x} - x_{d+1}) \tag{13}$$

Following the identification, the reflection point is expanded across the search space as given in Eq. (14):

$$x_e = \bar{x} + \gamma(x_r - \bar{x}) \tag{14}$$

where the expansion point is denoted by x_e which replaces the worst value if the value of the fitness for the expansion point is smaller than that of the reflection. Otherwise, x_r replaces this point. The contraction step is employed if the reflection point's fitness is bigger than that of the next worst. An outer contraction (x_{oc}) is generated by Eq. (15) to achieve the corresponding fitness value of $f(x_{oc})$ for $f(x_r) < f(x_{d+1})$.

$$x_{oc} = \bar{x} + \beta(x_r - \bar{x}) \tag{15}$$

The point of x_{oc} replaces the x_{d+1} point and the iterations are terminated if $f(x_{oc}) < f(x_r)$. Otherwise, the shrinkage occurs in the next action. An inner contraction (x_{ic}), provided in Eq. (16), may also be constructed in the contraction step in order to achieve corresponding fitness of $f(x_{ic})$ for $f(x_{d+1}) \leq f(x_r)$.

$$x_{ic} = \bar{x} + \beta(x_{d+1} - \bar{x}) \tag{16}$$

The point of x_{ic} replaces the x_{d+1} point and iterations are terminated in case of $f(x_{ic}) < f(x_{d+1})$, otherwise, the shrinkage occurs. The latter is similar to the case for outer contraction. The shrinkage step is the final operation in NM algorithm which uses Eq. (17) to construct new points by shrinking them.

$$x_i = x_1 + \delta(x_i - x_1), i = 2, 3, \cdots, d+1 \tag{17}$$

The flowchart of NM simplex method is provided in Fig. 3.

4. Proposed hybrid AEONM algorithm

The proposed hybrid AEONM algorithm aims to construct an efficient global optimization algorithm with balanced explorative and exploitative phases. Therefore, it employs good global search ability of AEO algorithm for exploration whereas the advantage of good local search capability of NM algorithm is used for exploitation. The AEO has a Lévy flight like behavior as can be seen from Eqs. (4) and (5), however, consists of a simpler structure which provides an enhanced exploration capability whereas NM is an algorithm that has greater exploitation ability. The complementary characteristics of AEO and NM is also the motivation of this study, thus, the constructed AEONM algorithm is proposed for the adjustment of PID controller employed in a buck converter.

The initialization of the proposed AEONM algorithm consists of setting the parameters of AEO algorithm (number of iterations, population size and number of decision variables) and NM simplex method (coefficients of ρ, γ, β, δ). The AEO algorithm is run to execute the exploration stage. The best solution obtained in this stage is used as the initial guess by the NM algorithm in order for execution of exploitation stage. The NM algorithm was run after every 10 iterations of AEO to perform the latter stage which allowed the algorithm to perform with the best efficiency. This continues through iterations until the stopping criterion is met. The flowchart of the proposed AEONM algorithm is given in Fig. 4.

In terms of initial performance assessment of the proposed AEONM algorithm, six well-known benchmark functions were adopted. The definitions and other details of those benchmark functions are presented in Table 1. To demonstrate a fair comparison, all algorithms (AEONM, AEO, PSO and DE) were run 25 times with a population size of 50 and a maximum iteration number of 1000.

The statistical results (best, mean and standard deviation) obtained for the relevant test functions using the compared algorithms are listed in Table 2. As can be seen from the numerical values demonstrated in Table 2, the best results were achieved with the proposed AEONM algorithm compared to the original AEO and other algorithms (PSO and DE). Considering the demonstrated success of the proposed AEONM algorithm in solving test functions, this study aims to further evaluate it comparatively in terms of solving a real-world engineering problem. The details of the relevant system and the respective performance analyses are all provided in the following sections.

5. Buck converter

5.1. Modeling of buck converter

The buck converter, also known as the step-down converter, is a nonlinear system that operates in switched mode, thus, presents a changing behavior with respect to time. Therefore, the linearized model of the converter must be derived first for designing a linear controller. The buck converter circuit and its small-signal model extracted from switching signal-flow graph (SFG) method [32] is shown in Fig. 5. The SFG method is a visible approach that allows obtaining the transfer function faster. The readers are referred to Refs. [32] and [33] for more details on SFG method.

The small-signal transfer function, from the control signal input to the capacitor voltage output, of the buck converter is obtained as in Eq. (18) by using the signal-flow graph in Fig. 5, graph algebra and Mason gain formula [34].

$$G_{vd}(s) = \frac{\hat{v}_o(s)}{\hat{d}(s)} = V_g \cdot \frac{\frac{1}{LC}}{s^2 + \frac{s}{RC} + \frac{1}{LC}} \tag{18}$$

The parameters of the step-down converter circuit are provided in Table 3 [11] where V_g is input voltage, R is load resistance, L is filter inductor, C is filter capacitor, V_{ref} is output voltage reference, D is steady-state duty cycle ratio and f_s is the switching frequency of the buck converter.

Using the values in the respective table, an open-loop step response of buck converter shown in Fig. 6 can be obtained which corresponds to a change of $\hat{d} = 1/12$ occurring in duty cycle ratio, hence, a change of 3 V in the output voltage. As can be seen from Fig. 6, the open loop response of the buck converter has a high overshoot value, and the settling time is quite long. Enhancement of those parameters is feasible via

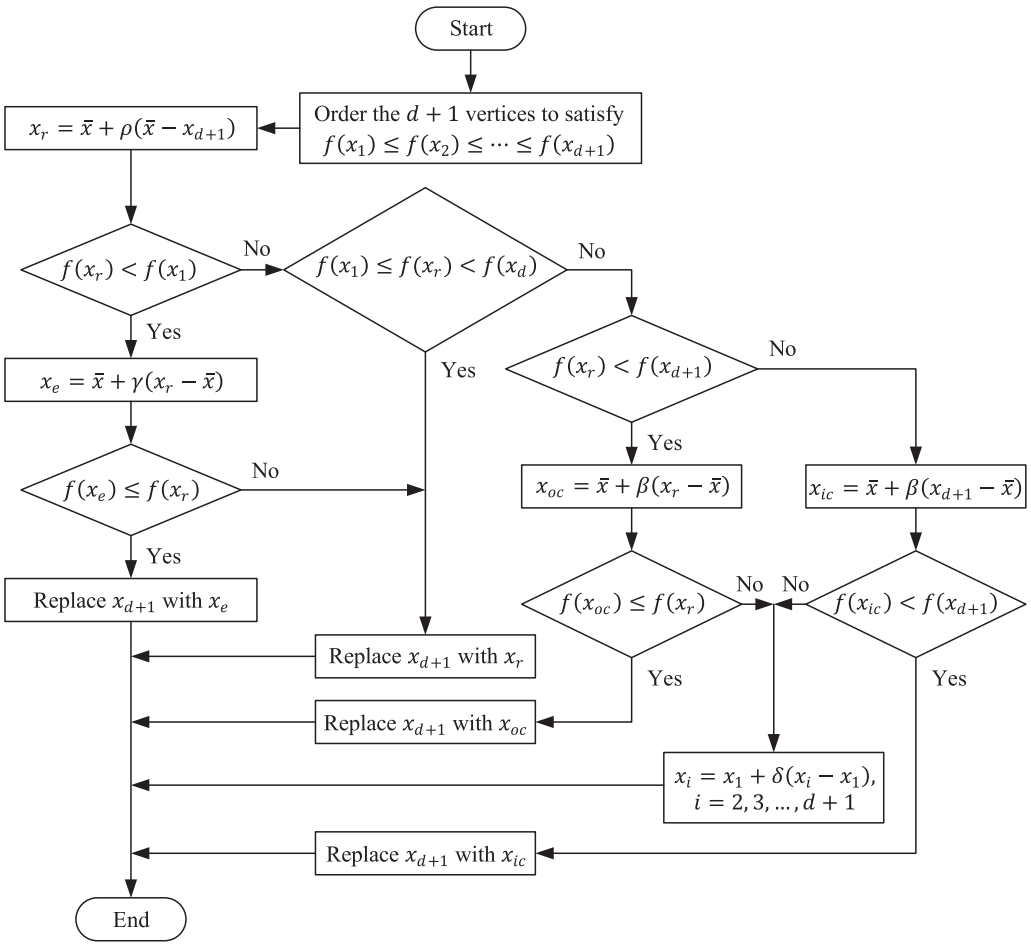

Fig. 3 Flowchart of NM simplex method.

employment of a PID controller as a simple and efficient structure. The respective controller is described in the following subsection.

5.2. PID controlled buck converter system

The transient response of the buck converter is stable even in the absence of a controller which is demonstrated in Fig. 6. However, it can also be seen that an improvement is required despite its stability. Therefore, in this study, closed loop control was performed via a PID controller to achieve an enhanced stability. The block diagram of the buck converter with PID controller is shown in Fig. 7.

The transfer function of PID controller is given in Eq. (19) whereas Eq. (20) provides the reference voltage to output voltage closed-loop transfer function of the buck converter:

$$G_{Controller}(s) = K_p + \frac{K_i}{s} + K_d s \tag{19}$$

$$T_{closed-loop}(s) = \frac{\hat{v}_o(s)}{\hat{v}_{ref}(s)} = \frac{G_{vd}(s) \times G_{Controller}(s)}{1 + G_{vd}(s) \times G_{Controller}(s)};\ \text{for}\ \hat{v}_{dist}(s) = 0 \tag{20}$$

where K_p, K_i and K_d are proportional, integral, and derivative gains of the controller, respectively. $\hat{v}_{ref}(s)$ denotes the reference voltage change whereas $\hat{v}_e(s)$ and $\hat{v}_o(s)$ are the error voltage and output voltage change, respectively. The unity feedback closed loop transfer function of the buck converter can be obtained as provided in Eq. (21) by substituting the system parameters listed in Table 3.

$$T_{closed-loop}(s) = \frac{216000 \cdot (K_d s^2 + K_p s + K_i)}{0.0006 s^3 + s^2 + 6000 s + 216000 \cdot (K_d s^2 + K_p s + K_i)} \tag{21}$$

It is worth to note that a linear controller design using the small signal model was considered in this study. Therefore, the controller output signals were assumed to be within reasonable limits which would not need to be limited by any means.

6. Definition of optimization problem and proposed design approach

The performance enhancement can be achieved by minimizing the maximum overshoot percentage, steady-state error, settling and rise times of the respective output voltage ($\hat{v}_o$) of the buck converter system via using an objective function F. In this study, the objective function proposed by Ref. [35] was employed which is given in Eq. (22):

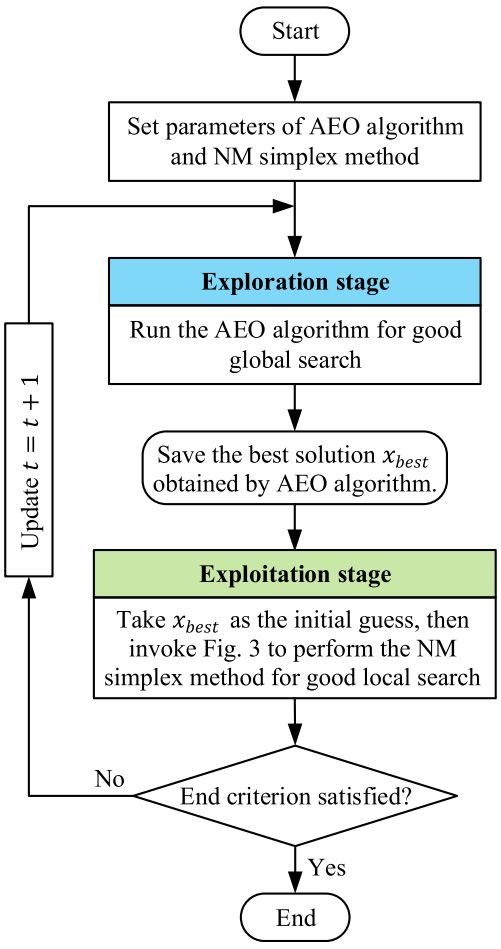

Fig. 4 Flowchart for the proposed AEONM algorithm.

$$F = (1 - e^{-\sigma}) \times \left(M_p + E_{ss}\right) + e^{-\sigma} \times (T_s - T_r) \tag{22}$$

where M_p is maximum overshoot percentage, E_{ss} is steady-state error, T_s is settling time and T_r is rise time. σ is the weighting coefficient, which is set as $5{\times}10^{-5}$ in this paper. After extensive simulations, the latter provided value of weighting coefficient has been found to be better if it is chosen within $\left[2 \times 10^{-5}, 10^{-4}\right]$ and the optimum value was determined to be 5×10^{-5}. It is worth to note that the proposed AEONM algorithm can find the best result for any σ value chosen from $\left[2 \times 10^{-5}, 10^{-4}\right]$. This objective function helps the output of the system to reach the steady-state value quickly without causing higher overshoots. In order to obtain a high level of dynamic performance from the buck converter, the K_p, K_i and K_d parameters should be set to their optimal values. The upper and lower limits of these parameters are given in Table 4 [10,36]. It is worth to note that the closed loop response of the system is always stable within the stated limits in Table 4. The detailed flowchart of the AEONM tuned PID controlled buck converter system to find optimal parameters is given in Fig. 8.

7. Simulation results and discussion

This section presents detailed comparative simulation results of the PID controlled buck converter systems designed with different approaches. The comparisons were performed by means of statistical boxplot analysis and non-parametric test results along with transient response analysis, frequency response analysis, integral error-based performance indices, disturbance rejection analysis and robustness analysis.

7.1. Compared algorithms

The proposed hybrid AEONM algorithm has been compared with the original AEO algorithm and the two other most popular algorithms (PSO and DE). The implementation of the AEO algorithm is quite simple such that it does not require any parameter adjustment apart from the numbers of population and the maximum iteration. The initial parameters of NM simplex method, PSO [37] and DE [38] algorithms are provided as follows.

NM: Reflection factor $\rho = 1$, expansion factor $\gamma = 2$, contraction factor $\beta = 0.5$ and shrinkage factor $\delta = 0.5$.
DE: Mutation factor $F = 0.5$ and crossover rate $C = 0.5$.
PSO: Inertia weight linearly reduces from 0.9 to 0.2, cognitive and social coefficients $c_1 = 2.0$ and $c_2 = 2.0$.

In each of the algorithms, the population number was set to 24 and the total number of iterations was taken as 50 and each of the algorithm was run 25 times.

7.2. Statistical boxplot analysis

The statistical performance of the proposed AEONM-based PID controller along with the other controllers based on AEO, PSO, and DE algorithms are given in this subsection. Table 5 presents the statistical results for the objective function F in terms of best, mean and standard deviation.

The respective values were ranked according to their statistical performances. From the table, the proposed AEONM

Table 1 Used benchmark functions.

Name	Formula	d	Test area	f_{opt}
Sphere	$f_1(x) = \sum_{i=1}^{d} x_i^2$	30	$[-100, 100]$	0
Schwefel 2.22	$f_2(x) = \sum_{i=1}^{d} \lvert x_i \rvert + \prod_{i=1}^{d} \lvert x_i \rvert$	30	$[-10, 10]$	0
Schwefel 1.2	$f_3(x) = \sum_{i=1}^{d} \left(\sum_{j=1}^{i} x_j\right)^2$	30	$[-100, 100]$	0
Schwefel 2.21	$f_4(x) = \max_i\{\lvert x_i \rvert, 1 \le i \le d\}$	30	$[-100, 100]$	0
Rosenbrock	$f_5(x) = \sum_{i=1}^{d-1} \left(100\left(x_{i+1} - x_i^2\right)^2 + \left(x_i - 1\right)^2\right)$	30	$[-30, 30]$	0
Ackley	$f_6(x) = -20exp\left(-0.2\sqrt{\frac{1}{d}\sum_{i=1}^{d} x_i^2}\right) - exp\left(\frac{1}{d}\sum_{i=1}^{d} cos(2\pi x_i)\right) + 20 + e$	30	$[-32, 32]$	0

Table 2 The comparison of the performances of AEONM, AEO, PSO and DE algorithms.

Name	Measure	AEONM (proposed)	AEO	PSO	DE
Sphere	Best	0	0	7.3467e−06	1.1883e−15
	Mean	0	0	2.1983e−04	3.5570e−14
	Standard deviation	0	0	2.5634e−04	6.2032e−14
Schwefel 2.22	Best	6.1797e−201	8.0628e−198	4.2105e−05	1.5396e−08
	Mean	2.8529e−190	1.1333e−189	3.0845e−04	4.1874e−08
	Standard deviation	0	0	2.4850e−04	2.4051e−08
Schwefel 1.2	Best	0	0	9.8861e+02	8.2076e−01
	Mean	0	0	2.7052e+03	5.4633e+00
	Standard deviation	0	0	1.2908e+03	3.5439e+00
Schwefel 2.21	Best	6.7214e−193	1.1256e−192	1.0485e+01	2.3077e+00
	Mean	4.9684e−186	6.0593e−184	1.6962e+01	9.2058e+00
	Standard deviation	0	0	4.0843e+00	4.0632e+00
Rosenbrock	Best	0	1.7923e+01	6.8303e+00	4.2950e+00
	Mean	3.5698e−29	1.9411e+01	9.7047e+01	3.1968e+01
	Standard deviation	5.0416e−29	9.5890e−01	7.5831e+01	1.7052e+01
Ackley	Best	8.8818e−16	8.8818e−16	9.3017e−04	1.8395e−08
	Mean	8.8818e−16	8.8818e−16	7.4902e−03	5.5394e−08
	Standard deviation	0	0	8.0841e−03	3.0611e−08

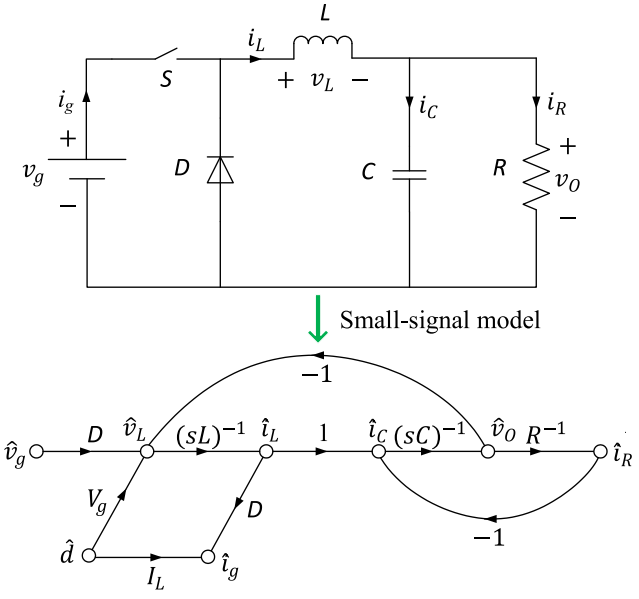

Fig. 5 Buck converter system and its small-signal model.

algorithm-based controller has ranked as first due to its superior performance over others in all parameters. These results can also be visualized through the comparative boxplot given in Fig. 9. Thus, the proposed AEONM algorithm-based controller design approach can be concluded to be better than of other algorithms-based design approaches.

7.3. Non-parametric test analysis

Apart from the statistical performance parameters provided in the previous section, a non-parametric statistical test based on the Wilcoxon signed-rank test was also performed to further demonstrate the superior performance of the proposed

Table 3 Parameters of the DC–DC buck converter used in simulation [11].

Parameters	Values
V_g	$36V$
V_{ref}	$12V$
R	6Ω
L	$1mH$
C	$100\mu F$
D	$1/3$
f_s	$40kHz$

AEONM algorithm. In this way, the superior performance of the proposed algorithm was shown not to be occurred by coincidence because of the stochastic nature of it. The non-parametric test was carried out at 5% significant level

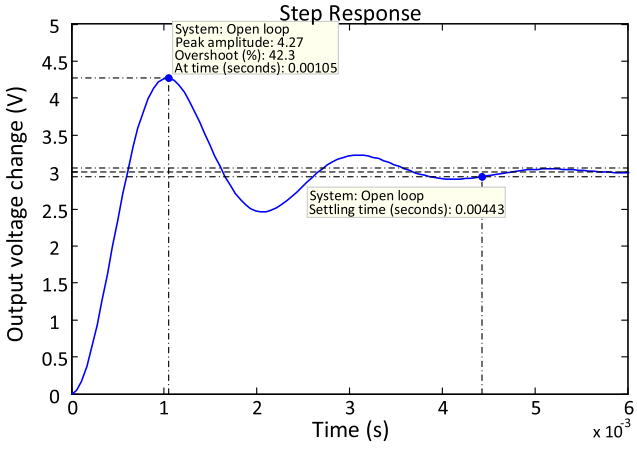

Fig. 6 Open-loop step response of buck converter.

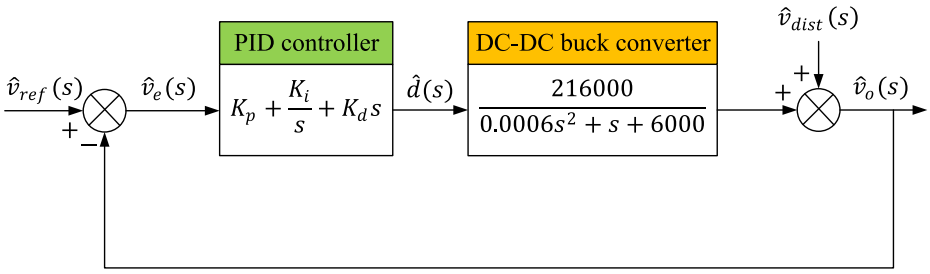

Fig. 7 Buck converter system with a PID controller.

Table 4 The limits of the PID parameters.

Parameter	Lower bound	Upper bound
K_p	1	50
K_i	0.01	10
K_d	0.001	0.01

AEONM versus other algorithms. The obtained p values are given in Table 6.

The obtained p values and the sign of $'+'$ in the winner column of the Table showed the significant difference of the proposed algorithm's performance compared to other algorithms, thereby, clearly demonstrating great effectiveness of the proposed AEONM algorithm with respect to AEO, PSO and DE algorithms.

7.4. Transient response analysis

The best controller parameters obtained with different algorithms in the optimization process are given in Table 7. Those parameters were used to observe the transient stability of the controlled system.

The respective closed loop transfer functions of the buck converter system tuned by the PID controller parameters provided in Table 7 are given in Eqs. (23)–(26) for AEONM, AEO, PSO and DE algorithms, respectively.

$$T_{AEONM}(s) = \frac{0.3571s^2 + 605.8s + 42.27}{1e-07s^3 + 0.3573s^2 + 606.8s + 42.27} \tag{23}$$

$$T_{AEO}(s) = \frac{0.3395s^2 + 1192s + 286.2}{1e-07s^3 + 0.3396s^2 + 1193s + 286.2} \tag{24}$$

$$T_{PSO}(s) = \frac{0.2956s^2 + 1337s + 134.1}{1e-07s^3 + 0.2957s^2 + 1338s + 134.1} \tag{25}$$

$$T_{DE}(s) = \frac{0.3143s^2 + 994.4s + 46.95}{1e-07s^3 + 0.3144s^2 + 995.4s + 46.95} \tag{26}$$

For the proposed AEONM/PID, AEO/PID, PSO/PID and DE/PID controller approaches, the comparative transient responses of the system with a reference voltage change of $\hat{v}_{ref} = 3$ V is shown in Fig. 10.

In addition, comparative numerical results in terms of important transient response performance criteria such as peak value, maximum overshoot, settling time, rise time and steady-state error are presented in Table 8. As can be seen from all these results, there is no overshoot in the system response with the proposed AEONM/PID controller and it is much faster which exhibits a more stable profile in time domain than other controllers. Hence, it is superior to other design approaches.

7.5. Frequency response analysis

Gain and phase margins along with bandwidth are the parameters that are important for the evaluation of the algorithms in the frequency domain. The Bode plot of the buck converter system using the controller (designed by the proposed approach) is shown in Fig. 11.

Table 9 shows the performance criteria of all approaches in frequency domain in terms of gain and phase margins as well as bandwidth. As can be clearly seen from the comparative numerical results in the table and the Bode plots from the figure, the most stable system in terms of frequency response is the one with the proposed AEONM/PID controller.

7.6. Comparison of time-domain integral-error-performance indices

This subsection presents a comparative analysis in terms of well-known integral of error-based performance indices which can be listed as IAE, ISE, ITAE, and ITSE which denote the integral of absolute error, integral of squared error, integral of time weighted absolute error, and integral of time weighted squared error, respectively. The formulations of the listed indices are given in Eqs. (27), (28), (29) and (30), respectively.

$$IAE = \int_0^T |e(t)| \cdot dt \tag{27}$$

$$ISE = \int_0^T e^2(t) \cdot dt \tag{28}$$

$$ITAE = \int_0^T t \cdot |e(t)| \cdot dt \tag{29}$$

$$ITSE = \int_0^T t \cdot e^2(t) \cdot dt \tag{30}$$

In the respective equations, T denotes the simulation time, which equals $10^{-5}s$ in this study, and $e(t)$ is the error signal that is given as $e(t) = \hat{v}_e = \hat{v}_{ref} - \hat{v}_o$. The values obtained from simulations for these indices are given as bar graphs in Figs. 12,

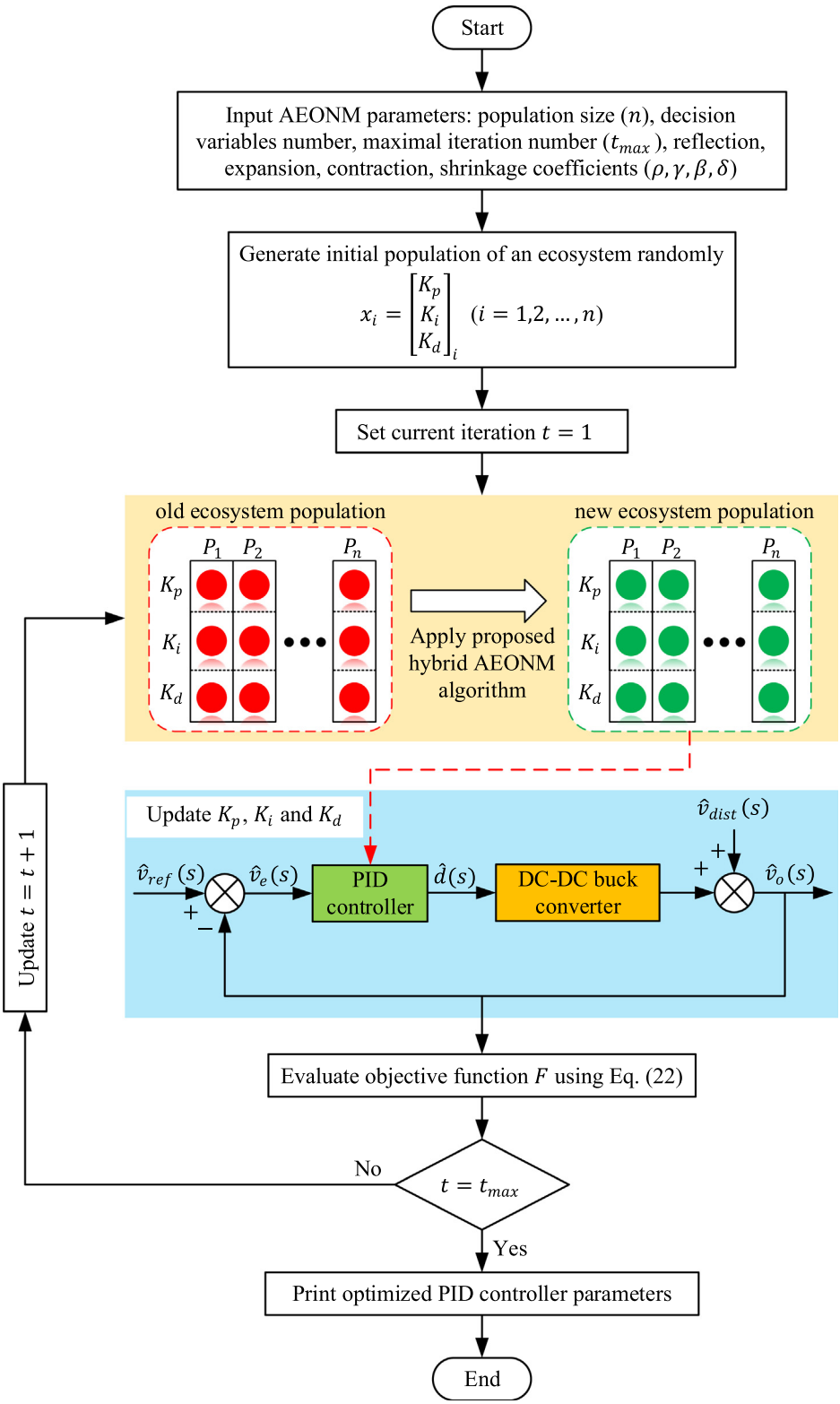

Fig. 8 Flowchart of the buck converter system with a PID controller tuned by suggested AEONM.

13, 14 and 15, respectively. It can be clearly seen from these figures that the proposed AEONM algorithm-based controller has provided the smallest value, indicating the best performance amongst all compared algorithms.

7.7. Disturbance rejection performance

This subsection presents the proposed AEONM-based controller's ability to reject the unexpected disturbances. The

Table 5 Comparison of statistical results for F objective function.

Algorithm	Best	Mean	Standard deviation	Rank
AEONM (proposed)	4.8016e−07	**4.9563e−07**	1.4493e−08	1
AEO	4.9920e−07	5.1693e−07	1.6234e−08	2
PSO	5.6805e−07	5.8939e−07	1.5587e−08	4
DE	5.6191e−07	5.8340e−07	1.9324e−08	3

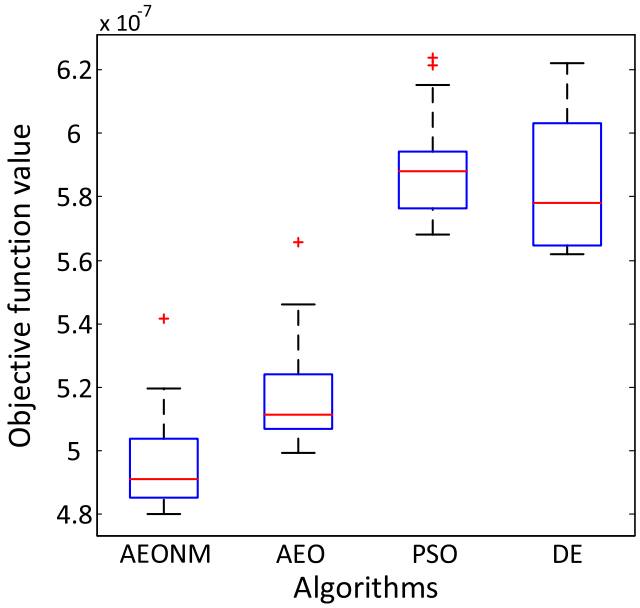

Fig. 9 Boxplot analysis results for AEONM, AEO, PSO and DE algorithms.

Table 6 Wilcoxon signed-rank test results for AEONM, AEO, PSO and DE algorithms.

Algorithm	p value	Winner
AEONM vs AEO	1.7437e − 04	+
AEONM vs PSO	1.2290e − 05	+
AEONM vs DE	1.2290e − 05	+

Table 7 PID controller parameters optimized by various algorithms.

Algorithm	K_p	K_i	K_d
AEONM (proposed)	16.8278	1.1742	0.00992
AEO	33.1153	7.9506	0.00943
PSO	37.1502	3.7255	0.00821
DE	27.6235	1.3043	0.00873

value of the disturbance signal was taken as the positive 20% change of the reference voltage change ($\hat{v}_{ref} = 3$ V) at $t = 5 \times 10^{-6}$ s. This sudden change in the output voltage caused by the disturbing effect and should be suppressed

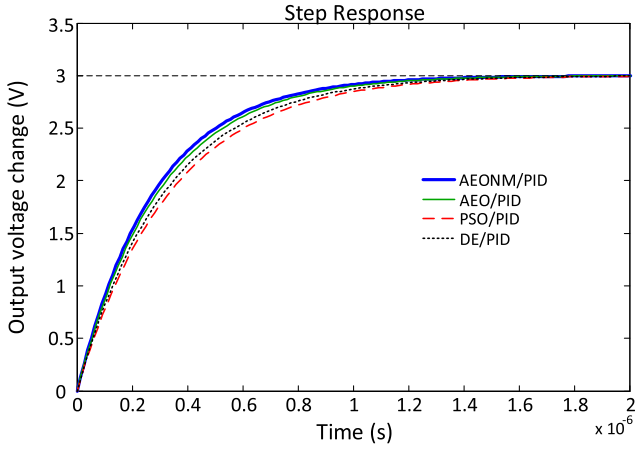

Fig. 10 Step response comparisons of the buck converter system.

quickly with the proposed controller. The response of the output voltage change ($\hat{v}_o$) due to the step input at $t = 0s$ and the response to the disturbance effect (0.6 V) at $t = 5 \times 10^{-6}s$ is shown in Fig. 16. From the figure, compared to AEO/PID, PSO/PID and DE/PID controllers, the proposed AEONM/PID controller is faster and better at suppressing the occurring disturbance.

7.8. Robustness analysis

The robustness of a controller is a crucial point to bear in mind in order to maintain the stability of the considered system for unexpected cases. The parameters of L and C were separately changed within a range of ±20% and ±10%, respectively, in order to perform the robustness analysis of the proposed AEONM based PID controller. Similar to the previous analyses, the robustness was also carried out comparatively against the PSO, DE and the original form of AEO algorithms. Table 10 provides the respective comparative results.

As can be seen from the results provided in Table 10, all algorithms provide zero steady-state error. However, in terms of other parameters of peak value, overshoot, rise and settling times, an overall superiority of the proposed approach can clearly be observed.

7.9. Comparison with the state-of-the-art algorithms

As part of further performance demonstration of the proposed approach for controlling buck converter, a comparison was performed in terms of transient and frequency responses

Table 8 Transient response performance of different algorithms.

Algorithm	Peak value (V)	Overshoot (%)	Rise time (s)	Settling time (s)	Steady-state error (V)
AEONM (proposed)	3.0000	0	6.1519e − 07	1.0954e − 06	0
AEO	3.0000	0	6.4613e − 07	1.1454e − 06	0
PSO	3.0000	0	7.4122e − 07	1.3093e − 06	0
DE	3.0013	0.0438	6.9808e − 07	1.2381e − 06	0

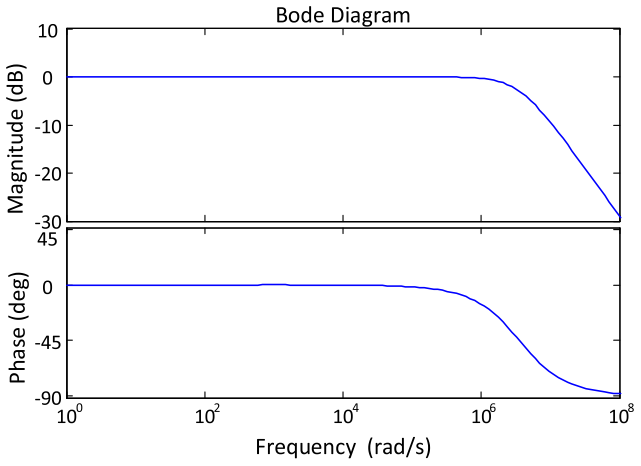

Fig. 11 Bode plot of the buck converter system with a PID controller tuned by proposed AEONM.

Table 9 Frequency response characteristics of different approaches.

Algorithm	Gain margin (dB)	Phase margin (deg)	Bandwidth (Hz)
AEONM (proposed)	infinite	180	3.5628e + 06
AEO	infinite	178.1149	3.3886e + 06
PSO	infinite	177.4863	2.9515e + 06
DE	infinite	178.2405	3.1369e + 06

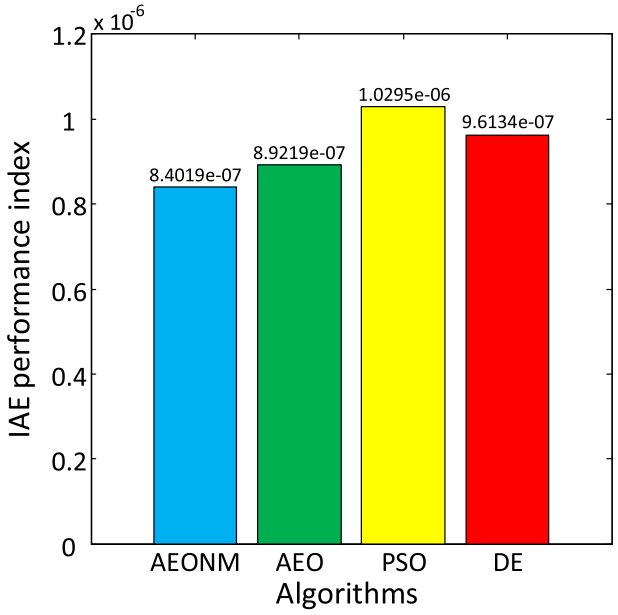

Fig. 12 Comparison of IAE performance index values.

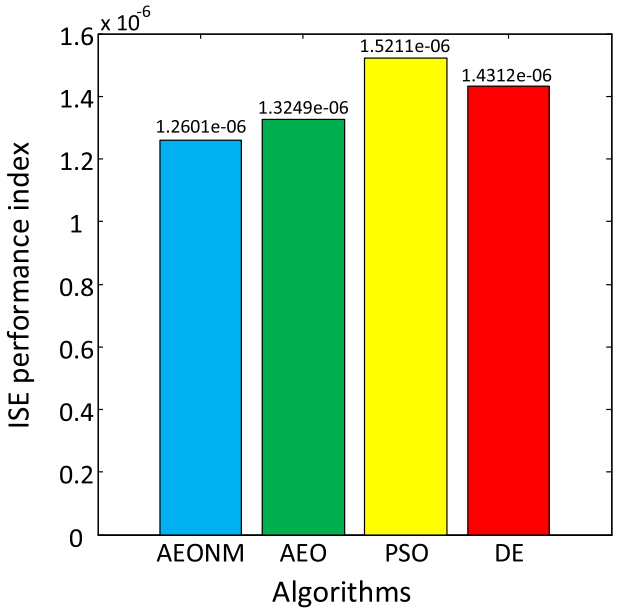

Fig. 13 Comparison of ISE performance index values.

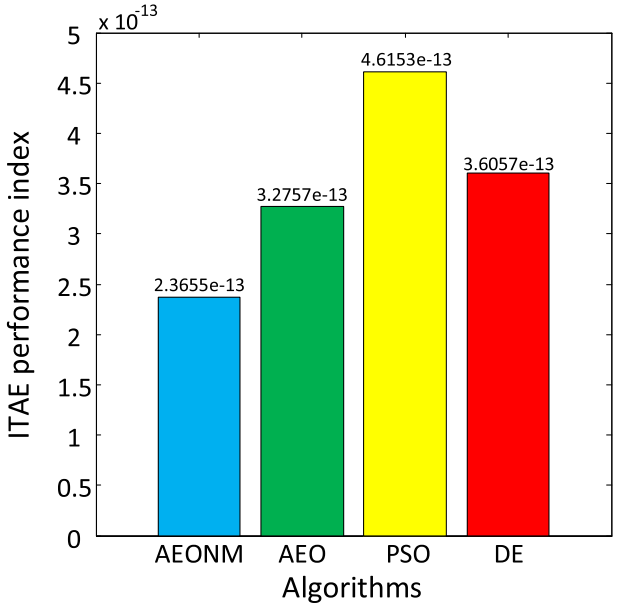

Fig. 14 Comparison of ITAE performance index values.

against SA, GA and WOA based controllers that were used for the same purpose. Table 11 presents the respective comparative values for all algorithms. The respective data shown in

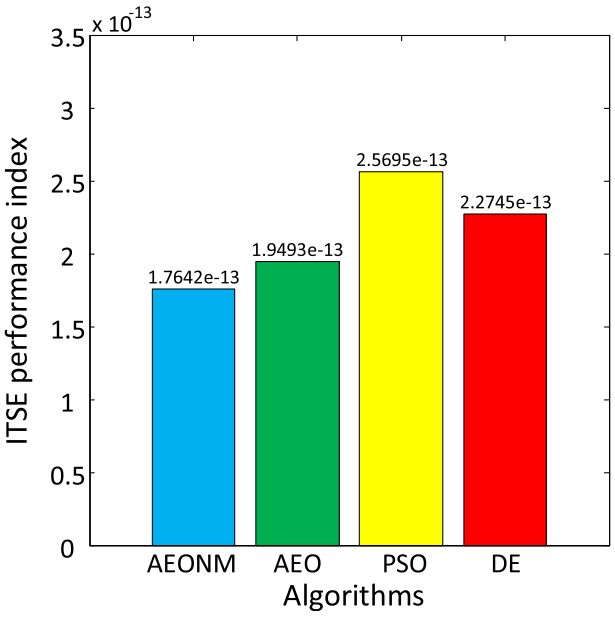

Fig. 15 Comparison of ITSE performance index values.

Table 11 demonstrates highly competitive capability of the proposed approach in terms of achieving good peak value, overshoot, rise time, settling time, steady-state error, gain margin, phase margin and bandwidth.

8. Conclusion

A new hybrid metaheuristic optimization algorithm, namely the artificial ecosystem-based optimization integrated with Nelder-Mead simplex method (AEONM), has been proposed for linear PID controller design of buck converter. After introduction of original optimization algorithms of AEO and NM, the proposed hybrid AEONM algorithm and its implementation to optimal PID controller design of buck converter has been described in detail. Initially, the proposed algorithm was tested against six well-known benchmark functions. Then, several analyses and time domain-based performance indices have been conducted to validate the efficiency of the proposed design approach and compared with not only the original AEO algorithm but also with other commonly used algorithms such as PSO and DE. According to the statistical test results in terms of best, mean, and standard deviation indices, the pro-

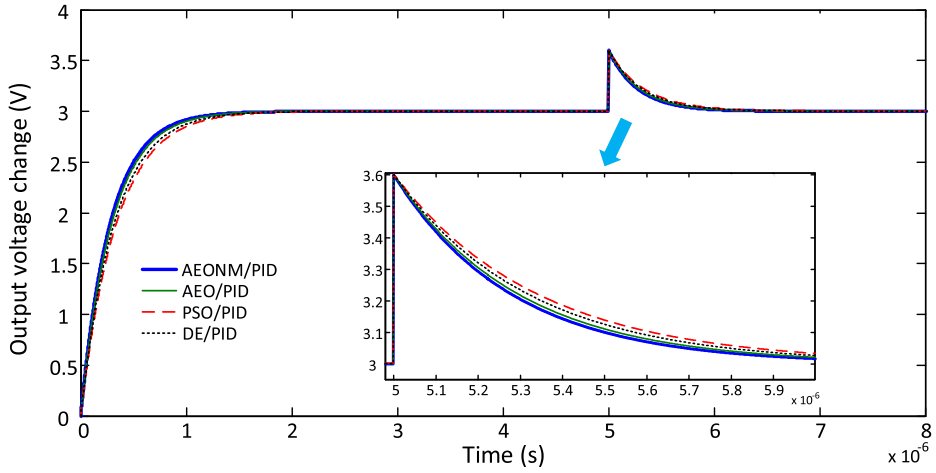

Fig. 16 Set point and disturbance responses of a DC–DC buck converter.

Table 10 Performance comparisons for parametric uncertainty.

Parameter	Rate of change	Algorithm	Peak value (V)	Overshoot (%)	Rise time (s)	Settling time (s)	Steady-state error (V)
L	−20%	AEONM	3.0000	0	4.9215e − 07	8.7631e − 07	0
		AEO	3.0012	0.0400	5.1707e − 07	9.1740e − 07	0
		PSO	3.0000	0	5.9331e − 07	1.0497e − 06	0
		DE	3.0010	0.0346	5.5862e − 07	9.9157e − 07	0
	+20%	AEONM	3.0000	0	7.3822e − 07	1.3144e − 06	0
		AEO	3.0000	0	7.7511e − 07	1.3727e − 06	0
		PSO	3.0003	0.0096	8.8896e − 07	1.5679e − 06	0
		DE	3.0000	0	8.3746e − 07	1.4842e − 06	0
C	−10%	AEONM	3.0000	0	5.5375e − 07	9.8636e − 07	0
		AEO	3.0012	0.0404	5.8170e − 07	1.0320e − 06	0
		PSO	3.0000	0	6.6740e − 07	1.1804e − 06	0
		DE	3.0010	0.0339	6.2846e − 07	1.1156e − 06	0
	+10%	AEONM	3.0001	0.0022	6.7661e − 07	1.2043e − 06	0
		AEO	3.0000	0	7.1053e − 07	1.2584e − 06	0
		PSO	3.0002	0.0058	8.1497e − 07	1.4379e − 06	0
		DE	3.0000	0	7.6766e − 07	1.3604e − 06	0

Table 11 Comparisons of the transient and frequency responses.

Performance criteria	AEONM (proposed)	SA [10]	GA [36]	WOA [36]
Peak value (V)	3.0000	3.0005	3.0000	3.0000
Overshoot (%)	0	0.0182	0	0
Rise time (s)	6.1519e − 07	7.7874e − 07	7.8296e − 07	6.4306e − 07
Settling time (s)	1.0954e − 06	1.3726e − 06	1.3883e − 06	1.1391e − 06
Steady-state error (V)	0	0	0	0
Gain margin (dB)	infinite	infinite	infinite	infinite
Phase margin (deg)	180	177.1461	178.1775	177.9724
Bandwidth (Hz)	3.5628e + 06	2.8077e + 06	2.7966e + 06	3.4042e + 06

posed AEONM algorithm-based design approach ranked first in all these terms. Also, a non-parametric analysis based on the Wilcoxon signed-rank test has been conducted to show that the high performance of the proposed AEONM algorithm has not been occurred by coincidence. The obtained results from this test have clearly demonstrated the effectiveness of the proposed AEONM algorithm with respect to AEO, PSO, and DE algorithms. According to the transient response analysis results, the proposed design had no overshoot and no steady-state error, and the responses are much faster than the other design approaches with less rise time and settling time. The frequency response analysis has given similar high-performance results in terms of gain margin, phase margin and bandwidth. Both the tabulated numerical results and graphical Bode plot results have shown that the proposed AEONM-based design approach is superior to other design approaches. These results are also validated through four different time-domain integral-error performance indices, namely the IAE, ISE, ITAE, and ITSE, in which AEONM based design approach has given the minimum (best) results in all these performance indices. From the disturbance rejection analysis, it is shown that the PID controller design based on the proposed AEONM algorithm has better disturbance rejection capability than other design approaches with a higher disturbance suppression speed. Moreover, the robustness analysis has also shown the greater capability of the proposed approach. Lastly, a comparative analysis, in terms of transient and frequency responses, against SA [10], GA [36] and WOA [36] based PID controllers have also demonstrated the better performance of the proposed approach for control of DC-DC buck converter. Therefore, from all these analyses results, it can be concluded that the proposed hybrid optimization algorithm is an efficient design tool that can be used to design controllers in control applications of electrical engineering field which can be the subject of future research studies of controller designs for different engineering systems such as automatic voltage regulator, DC motor speed control, power system stabilizer and so on. The codes of the proposed algorithm written in MATLAB environment can be accessed at "https://github.com/davutizci/AEONM-Algorithm".

Declaration of Competing Interest

The authors declare that they have no known competing financial interests or personal relationships that could have appeared to influence the work reported in this paper.

References

[1] J. Li, A. Wu, Influence of non-ideal factors on the boundary control of buck converters with curved switching surfaces, IEEE Access 7 (2019) 52790–52803, https://doi.org/10.1109/Access.628763910.1109/ACCESS.2019.2912449.

[2] R. Sheehan, L. Diana, Switch-mode power converter compensation made easy, in: Texas Instruments Power Supply Des. Semin., Texas Instruments, 2016. https://www.ti.com/seclit/ml/slup340/slup340.pdf.

[3] A.G. Soriano-Sánchez, M.A. Rodríguez-Licea, F.J. Pérez-Pinal, J.A. Vázquez-López, Fractional-order approximation and synthesis of a PID controller for a buck converter, Energies 13 (3) (2020) 629, https://doi.org/10.3390/en13030629.

[4] S. Kapat, P.T. Krein, A tutorial and review discussion of modulation, control and tuning of high-performance DC-DC converters based on small-signal and large-signal approaches, IEEE Open J. Power Electron. 1 (2020) 339–371, https://doi.org/10.1109/OJPEL10.1109/OJPEL.2020.3018311.

[5] M. Leng, G. Zhou, Q. Tian, G. Xu, X. Zhang, Improved small-signal model for switching converter with ripple-based control, IEEE Trans. Ind. Electron. 68 (1) (2021) 222–235, https://doi.org/10.1109/TIE.4110.1109/TIE.2020.2965478.

[6] A.M. Bozorgi, V. Fereshtehpoor, M. Monfared, N. Namjoo, Controller design using ant colony algorithm for a non-inverting buck-boost chopper based on a detailed average model, Electr. Power Components Syst. 43 (2) (2015) 177–188, https://doi.org/10.1080/15325008.2014.975385.

[7] M. Mini, L.P. Suresh, Comparative Evaluation of Bio-inspired Controller for a Buck-Boost Converter, Aust. J. Basic Appl. Sci. 9 (2015) 361–366. http://www.ajbasweb.com/old/ajbas/2015/Special ICSCS/361-366.pdf.

[8] G. Tulay, İ. İskender, H. Erdem, Optimal tuning of a boost PFC converter PI controller using heuristic optimization methods, Int. Trans. Electr. Energy Syst. 27 (2017), https://doi.org/10.1002/etep.2458 e2458.

[9] S. Banerjee, A. Ghosh, N. Rana, An Improved Interleaved Boost Converter with PSO-Based Optimal Type-III Controller, IEEE J. Emerg. Sel. Top. Power Electron. 5 (1) (2017) 323–337, https://doi.org/10.1109/JESTPE.2016.2608504.

[10] B. Hekimoglu, S. Ekinci, Optimally designed PID controller for a DC-DC buck converter via a hybrid whale optimization algorithm with simulated annealing, Electrica 20 (1) (2020) 19–27, https://doi.org/10.5152/electrica.10.5152/electrica.202010.5152/electrica.2020.19034.

[11] S. Ekinci, B. Hekimoglu, E. Eker, D. Sevim, Hybrid Firefly and Particle Swarm Optimization Algorithm for PID Controller Design of Buck Converter, in: 3rd Int. Symp. Multidiscip. Stud. Innov. Technol. ISMSIT 2019 - Proc., 2019: pp. 1–6. https://doi.org/10.1109/ISMSIT.2019.8932733.

[12] D. Izci, S. Ekinci, S. Orenc, A. Demiroren, Improved artificial electric field algorithm using Nelder-mead simplex method for optimization problems, in: 2020 4th Int. Symp. Multidiscip. Stud. Innov. Technol., IEEE, 2020, pp. 1–5. https://doi.org/10.1109/ISMSIT50672.2020.9255255.
[13] W. Zhao, L. Wang, Z. Zhang, Artificial ecosystem-based optimization: a novel nature-inspired meta-heuristic algorithm, Neural Comput. Appl. 32 (13) (2020) 9383–9425, https://doi.org/10.1007/s00521-019-04452-x.
[14] D. Yousri, H. Rezk, A. Fathy, Identifying the parameters of different configurations of photovoltaic models based on recent artificial ecosystem-based optimization approach, Int. J. Energy Res. 44 (14) (2020) 11302–11322, https://doi.org/10.1002/er.v44.1410.1002/er.5747.
[15] A. S. Menesy, H.M. Sultan, A. Korashy, F.A. Banakhr, M. G. Ashmawy, S. Kamel, Effective parameter extraction of different polymer electrolyte membrane fuel cell stack models using a modified artificial ecosystem optimization algorithm, IEEE Access 8 (2020) 31892–31909, https://doi.org/10.1109/Access.628763910.1109/ACCESS.2020.2973351.
[16] R.M. Rizk-Allah, A.A. El-Fergany, Artificial ecosystem optimizer for parameters identification of proton exchange membrane fuel cells model, Int. J. Hydrogen Energy (2020), https://doi.org/10.1016/j.ijhydene.2020.06.256.
[17] A.T. Sahlol, M. Abd Elaziz, A. Tariq Jamal, R. Damaševičius, O. Farouk Hassan, A novel method for detection of tuberculosis in chest radiographs using artificial ecosystem-based optimisation of deep neural network features, Symmetry (Basel). 12 (7) (2020) 1146, https://doi.org/10.3390/sym12071146.
[18] A. Eid, S. Kamel, A. Korashy, T. Khurshaid, An enhanced artificial ecosystem-based optimization for optimal allocation of multiple distributed generations, IEEE Access 8 (2020) 178493–178513, https://doi.org/10.1109/Access.628763910.1109/ACCESS.2020.3027654.
[19] S. Mouassa, F. Jurado, T. Bouktir, M.A.Z. Raja, Novel design of artificial ecosystem optimizer for large-scale optimal reactive power dispatch problem with application to Algerian electricity grid, Neural Comput. Appl. 33 (13) (2021) 7467–7490, https://doi.org/10.1007/s00521-020-05496-0.
[20] H.M. Sultan, A.S. Menesy, S. Kamel, A. Korashy, S.A. Almohaimeed, M. Abdel-Akher, An improved artificial ecosystem optimization algorithm for optimal configuration of a hybrid PV/WT/FC energy system, Alexandria Eng. J. 60 (1) (2021) 1001–1025, https://doi.org/10.1016/j.aej.2020.10.027.
[21] J.A. Nelder, R. Mead, A simplex method for function minimization, Comput. J. 7 (4) (1965) 308–313, https://doi.org/10.1093/comjnl/7.4.308.
[22] B.K. Panigrahi, V. Ravikumar Pandi, Bacterial foraging optimisation: Nelder-Mead hybrid algorithm for economic load dispatch, IET Gener. Transm. Distrib. 2 (2008) 556–565, https://doi.org/10.1049/iet-gtd:20070422.
[23] L. Wang, Y.e. Xu, L. Li, Parameter identification of chaotic systems by hybrid Nelder-Mead simplex search and differential evolution algorithm, Expert Syst. Appl. 38 (4) (2011) 3238–3245, https://doi.org/10.1016/j.eswa.2010.08.110.
[24] A. Rajan, T. Malakar, Optimal reactive power dispatch using hybrid Nelder-Mead simplex based firefly algorithm, Int. J. Electr. Power Energy Syst. 66 (2015) 9–24, https://doi.org/10.1016/j.ijepes.2014.10.041.
[25] A.R. Yildiz, E. Kurtulus, E. Demirci, B.S. Yildiz, S. Karagoz, Optimization of thin-wall structures using hybrid gravitational search and nelder-Mead algorithm, Mater. Test. 58 (2016) 75–78, https://doi.org/10.3139/120.110823.
[26] J. Senthil Kumar, S. Charles Raja, J. Jeslin Drusila Nesamalar, P. Venkatesh, Optimizing renewable based generations in AC/DC microgrid system using hybrid Nelder-Mead – Cuckoo Search algorithm, Energy 158 (2018) 204–215, https://doi.org/10.1016/j.energy.2018.06.029.
[27] S. Xu, Y. Wang, Z. Wang, Parameter estimation of proton exchange membrane fuel cells using eagle strategy based on JAYA algorithm and Nelder-Mead simplex method, Energy 173 (2019) 457–467, https://doi.org/10.1016/j.energy.2019.02.106.
[28] A.R. Yıldız, B.S. Yıldız, S.M. Sait, S. Bureerat, N. Pholdee, A new hybrid Harris hawks-Nelder-Mead optimization algorithm for solving design and manufacturing problems, Mater. Test. 61 (2019) 735–743, https://doi.org/10.3139/120.111378.
[29] J. Xu, F.u. Yan, Hybrid Nelder-mead algorithm and dragonfly algorithm for function optimization and the training of a multilayer perceptron, Arab. J. Sci. Eng. 44 (4) (2019) 3473–3487, https://doi.org/10.1007/s13369-018-3536-0.
[30] H.N. Fakhouri, A. Hudaib, A. Sleit, Hybrid particle swarm optimization with sine cosine algorithm and Nelder-mead simplex for solving engineering design problems, Arab. J. Sci. Eng. 45 (4) (2020) 3091–3109, https://doi.org/10.1007/s13369-019-04285-9.
[31] J.C. Lagarias, J.A. Reeds, M.H. Wright, P.E. Wright, Convergence properties of the Nelder-Mead simplex method in low dimensions, SIAM J. Optim. 9 (1) (1998) 112–147, https://doi.org/10.1137/S1052623496303470.
[32] K. Smedley, S. Cuk, Switching flow-graph nonlinear modeling technique, IEEE Trans. Power Electron. 9 (4) (1994) 405–413, https://doi.org/10.1109/TPEL.6310.1109/63.318899.
[33] B. Hekimoğlu, S. Ekinci, Nonlinear modeling and simulation of DC-DC buck converter using switching flow-graph method, DUMF J. Eng. 9 (2018) 51–60. https://dergipark.org.tr/tr/pub/dumf/issue/36316/412400.
[34] B.C. Kuo, Automatic Control Systems, eighth ed., John Wiley & Sons, New York, 2003.
[35] Z.-L. Gaing, A particle swarm optimization approach for optimum design of PID controller in AVR system, IEEE Trans. Energy Convers. 19 (2) (2004) 384–391, https://doi.org/10.1109/TEC.2003.821821.
[36] B. Hekimoğlu, S. Ekinci, S. Kaya, Optimal PID Controller Design of DC-DC Buck Converter using Whale Optimization Algorithm, in: 2018 Int. Conf. Artif. Intell. Data Process. IDAP 2018, 2019, pp. 1–6. https://doi.org/10.1109/IDAP.2018.8620833.
[37] J. Kennedy, R. Eberhart, Particle swarm optimization, in: Proc. ICNN'95-International Conf. Neural Networks, IEEE, 1995, pp. 1942–1948.
[38] R. Storn, K. Price, Differential evolution - a simple and efficient heuristic for global optimization over continuous spaces, J. Glob. Optim. 11 (1997) 341–359, https://doi.org/10.1023/A:1008202821328.